IEEE Photonics Journal
An IEEE Photonics Society Publication

Open Access

High Precision Dual Frequency Doppler Lidar Based on Monolithic Integrated Two-Section DFB Lasers

Volume 11, Number 6, December 2019

Zuye Lu
Yunshan Zhang
Jie Zeng
Lianyan Li
Bocheng Yuan
Yuechun Shi
Jilin Zheng
Zijun Shang
Rulei Xiao
Tao Fang
Xiangfei Chen, *Senior Member, IEEE*

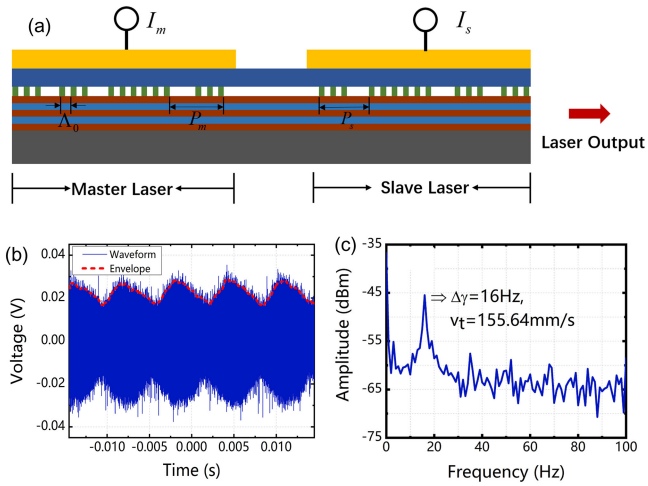

DOI: 10.1109/JPHOT.2019.2950289

High Precision Dual Frequency Doppler Lidar Based on Monolithic Integrated Two-Section DFB Lasers

Zuye Lu,[1] Yunshan Zhang,[2] Jie Zeng,[1] Lianyan Li,[2] Bocheng Yuan,[2] Yuechun Shi,[1,4] Jilin Zheng,[3] Zijun Shang,[2] Rulei Xiao,[1] Tao Fang,[1] and Xiangfei Chen,[1] *Senior Member, IEEE*

[1]College of Engineering and Applied Sciences, Nanjing University, Nanjing 210093, China
[2]School of Optoelectronic Engineering, Nanjing University of Posts and Telecommunications, Nanjing 210023, China
[3]Photonics Information Technology Laboratory, Institute of Communication Engineering, Army Engineering University of PLA, Nanjing 210007, China
[4]Nanjing University High-Tech Institute at Suzhou, Suzhou 215123, China

DOI:10.1109/JPHOT.2019.2950289

Manuscript received September 24, 2019; revised October 18, 2019; accepted October 24, 2019. Date of publication October 29, 2019; date of current version November 26, 2019. This work was supported in part by Chinese National Key Basic Research Special Fund under Grant 2017YFA0206401, in part by Jiangsu Science and Technology Project under Grant BE2017003-2, in part by the Nature Science Foundation of Jiangsu Province of China under Grant BK20160907, in part by Suzhou Technological Innovation of Key Industries under Grant SYG201844, in part by Open Foundation of Research Center of Optical Communications Engineering and Technology, and in part by Jiangsu Province under Grant ZXF20170302. Corresponding author: Yunshan Zhang (e-mail: yszhang@njupt.edu.cn).

Abstract: A dual-frequency Doppler Lidar (DFDL) with high precision utilizing a monolithic integrated two-section DFB laser as the dual-frequency light source is proposed and experimentally demonstrated. The DFDL can be realized with smaller size using the monolithic integrated two-section DFB laser which is fabricated by the reconstruction-equivalent-chirp (REC) technique with high precision and low fabrication cost. The range of the measured speed is from 13.62 μm /s to 1.56 m/s, which covers 6 orders of magnitude. The largest relative error of the DFDL system is 3.16%. The DFDL system has an excellent resolution of 1.95 μm/s, which is suitable to detect micro speed changes.

Index Terms: Semiconductor lasers, integrated photonic systems.

1. Introduction

Lidar (Light Detection And Ranging) systems are commonly applied to monitoring fauna dispersal in aquatic environments [1], urban land cover classification [2], aircraft wake vortex light detection [3], remote sensing in the atmosphere [4] and road traffic detection [5].Comparing to traditional radar (radio detection and ranging), lidar has advantages when high directionality, high spatial resolution, and noninvasive detection capabilities are required [6]. The speed of the moving target can be directly measured using the coherent lidar system by detecting the Doppler shift of the beam scattered from the target [6]. However, the measurement accuracy of the traditional single-frequency Doppler lidar (SFDL) is easily affected by the scattering of the laser emission from a rough surface, which leads to a speckle effect that modulates the Doppler signal causing broadening of the signal spectrum. Consequently, the accuracy of the velocity measurement is deteriorated [7]. In addition,

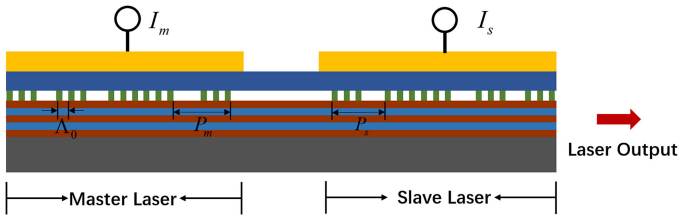

Fig. 1. The schematic of the two-section DFB laser.

the velocity measurement accuracy is also determined by the linewidth of the light source and the higher the measurement precision, the narrower the line width is required [8].

The dual-frequency Doppler lidar (DFDL) is an alternative approach to solve above issues [9]–[13]. With a microwave beat signal carried by the light, the DFDL has the advantage of good directionality, high intensity, high spatial resolution from the light, low speckle noise and good coherence from the microwave [13]. By phase-locking of the dual-frequency light source with a microwave signal, the coherence of the light source can be further improved and the detection range of the DFDL can be extended significantly [13]. Furthermore, the differential Doppler shift measurement based on the beating signal of the dual-frequency light reduces the requirement on the linewidth and improves the robustness and accuracy of the DFDL [13]–[15].

Traditionally, optically-injected semiconductor lasers or mode-locked lasers are utilized as the dual-frequency light source in the DFDL systems [16], [17]. Commonly, the optically-injected semiconductor lasers and mode-locked lasers consist of many discrete devices, which are sophisticated and very expensive. Consequently, the application of the DFDL systems is restricted significantly. Therefore, the DFDL systems with simple integrated light source are also desired.

In this paper, a DFDL system utilizing a monolithic integrated two-section DFB laser as the light source is presented. The two-section DFB laser is designed by the reconstruction-equivalent chirp (REC) technique, which can provide good single longitudinal mode (SLM) operation and precisely controlled wavelength with low fabrication costs [18], [19]. A microwave beat signal of 15.42 GHz is generated by the two modes of the two-section DFB laser. An external RF signal is injected into the slave laser to synchronize the two modes, which can enhance the coherence of the two-section DFB laser. Using the DFDL system, different speeds ranging from 13.62 μm /s to 1.56 m/s are measured with relative error less than 3.16%. The proposed DFDL measurement system has an excellent resolution of 1.95 μm/s, which can be used to detect micro speed changes.

2. Experimental Principle and Setup

2.1 Device Design

The DFDL system uses a monolithic integrated two-section DFB laser as the light source. Fig. 1 shows the schematic of the monolithic integrated two-section DFB laser. It consists of two in-line DFB lasers, which are called the master laser (ML) and the slave laser (SL) respectively. The cavity lengths of the two sections are both 650 μm and they share a common active layer. The epitaxy of the device is grown by conventional two-stage metal organic chemical vapor deposition (MOCVD) on an n-InP substrate. An n-InP buffer layer, an n-InAlGaAs lower optical confinement layer, an InAlGaAs multiple-quantum-well structure, a p-InGaAsP upper optical confinement layer and a p-InGaAsP grating layer are successively grown on an n-InP substrate in the first epitaxial growth. The sampled grating is fabricated by a conventional holographic exposure combining with conventional photolithography. After the fabrication of the sampled grating, a p-InP cladding layer and a p-InGaAs contact layer are successively regrown over the entire structure in the second epitaxial growth. Then the ridge waveguides are processed on the second epitaxial layers and p-metal contact windows are opened for metallization. The ML and SL are electrically isolated with each other by removing a small area of the highly p-doped InGaAs contact layer between the two sections.

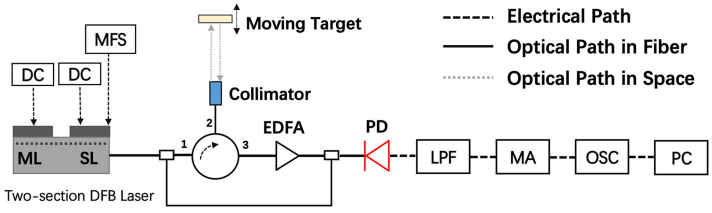

Fig. 2. The schematic of experment setup. MFS: microwave frequency synthesizer; EDFA: erbium-doped fiber amplifier; PD: photodetector; LPF: low-pass filter; MA: microwave amplifier; OSC: oscilloscope; PC: computer.

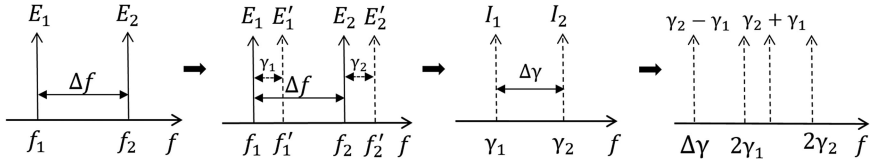

Fig. 3. The brief principle of the DFDL system.

Finally, both facets of the devices are coated by anti-reflection (AR) coatings with reflectivity less than 1% to suppress the Fabry–Perot modes of the lasers [18].

The gratings are designed by the REC technique with an identical seed grating period $\Lambda_0 = 256$ nm. We employ equivalent phase shifts in the gratings to ensure good SLM operation, and control the lasing wavelength by changing the sampling period P_m and P_s [19]. Through tuning the sampling periods, the wavelengths of the two lasers and the detuning frequency can be controlled accurately with the largest deviation less than 0.2 nm [20], which is sufficient for the generation of two mode. In order to obtain a detuning frequency near 50 GHz, the sampling period of P_m and P_s are set at 4.29 μm and 4.32 μm respectively. Furtherly, the detuning frequency between the two modes can be adjusted more finely by changing the bias current of ML and SL, which is denoted by I_m and I_s.

2.2 Experiment Setup and Theory Principle

Fig. 2 shows the schematic of experiment setup and Fig. 3 shows the brief principle of the DFDL system. The working temperature of two-section DFB laser was controlled at 25 °C by a thermal-electronic cooler (TEC). The ML and SL are biased at I_m and I_s separately by the DC current drivers, and the SL is modulated by a RF signal to narrow the linewidth of the dual-mode beating signal. The dual-mode light is generated by the two-section DFB laser, which contains two different frequency components, f_1 and f_2. In the system, the light source can be expressed as [9]:

$$E(t) = E_1(t) + E_2(t) = A_1 \exp[2\pi f_1 t + \varphi_1(t)] + A_2 \exp[2\pi f_2 t + \varphi_2(t)] \quad (1)$$

where E_1 and E_2 represent electrical fields of two modes, A_i and $\varphi_i(t)$ respectively represent the amplitude and phase of mode-i.

The synchronized dual-mode light is sent to port-1 of a circulator and then the light is transmitted through the collimator in the port-2 to the moving target. The back-reflected light with Doppler shift is coupled to the circulator by the same collimator. The back-reflected is injected to an erbium-doped fiber amplifier (EDFA) through the port-3 of the circulator. When the light signal is back-reflected by the moving target, each mode add the Doppler shift. Consequently, the f_1 and f_2 change to $f_1' = f_1 + \gamma_1$ and $f_2' = f_2 + \gamma_2$ respectively, where $\gamma_i = 2v_t f_i / c$ is the Doppler frequency shift, v_t is the speed of the moving target, c is the speed of light.

The back-reflected light coupling with the reference light is detected by a photodetector. The mixing signal from the photodetector is transmitted through a low-pass filter and a microwave

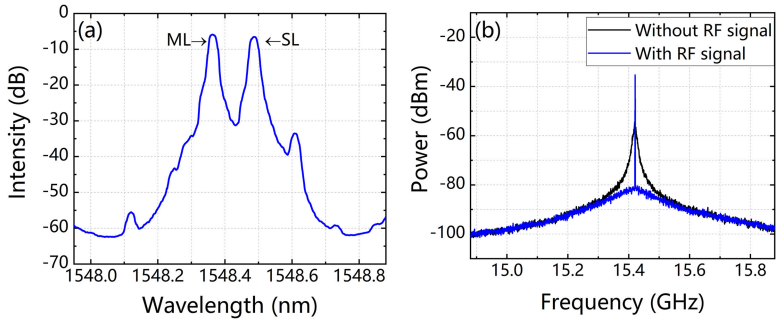

Fig. 4. (a) The optical spectrum of the two-section DFB laser working in the dual-mode state. Drive currents are set at $I_s = 50$ mA and $I_m = 70$ mA. (b) The electronic spectrum of the beat signal with and without RF signal.

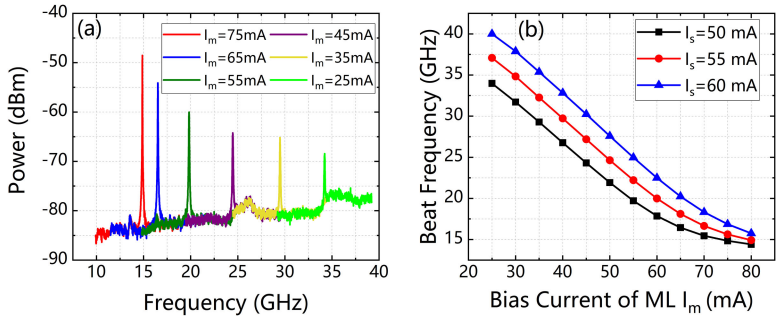

Fig. 5. (a) Electrical spectra of the beat signals when I_s is fixed at 50 mA and I_m varies from 25 mA to 75 mA. (b) The range of the beat frequency when I_s varies from 50 mA to 60 mA.

amplifier. By filtering out the high frequency components through the filter, the signal from the photodetector is expressed as [9]:

$$I_m(t) = 4C_1C_2\cos\left[2\pi\left(\gamma_2 - \gamma_1\right)t - 2\pi\Delta f\tau + \varphi_1\left(t-\tau\right) + \varphi_2\left(t-\tau\right) - \varphi_1\left(t\right) - \varphi_2\left(t\right)\right]. \quad (2)$$

Then the mixing signal is acquired by a real-time oscilloscope (OSC) and analyzed by a computer. The velocity of the moving target is:

$$v_t = \Delta\gamma \cdot c/2\Delta f \quad (3)$$

Where $\Delta\gamma = \gamma_2 - \gamma_1$ and $\Delta f = |f_1 - f_2|$ is the beating frequency of the dual laser modes.

3. Result

Fig. 4(a) shows the optical spectra of the main mode of SL and ML, when the drive currents of SL and ML are set at $I_s = 50$ mA and $I_m = 70$ mA respectively. The frequency difference between the SL and ML is $\Delta f = 15.42$ GHz. The external RF signal generated by microwave frequency synthesizer (MFS) with frequency of 15.42 GHz is injected into the SL to enhance the phase synchronization of the two modes. Fig. 4(b) shows the electronic spectrum of the beat signal with and without RF signal. It can be seen that the beat signal with RF signal has a very narrow linewidth comparing with original beat signal.

The beat frequency (i.e., the detuning frequency between the two modes) can be tuned by changing the bias currents of the ML and SL. Fig. 5(a) shows the electrical spectra of the beat signals with different currents. It is obvious that the beat frequency varies with the bias currents of

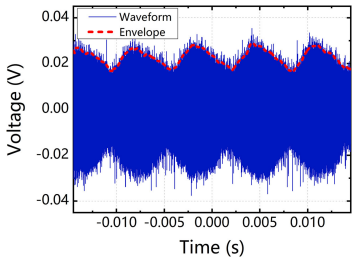

Fig. 6. The waveform data obtained by the real time oscilloscope, the red dotted line is envelope of the waveform.

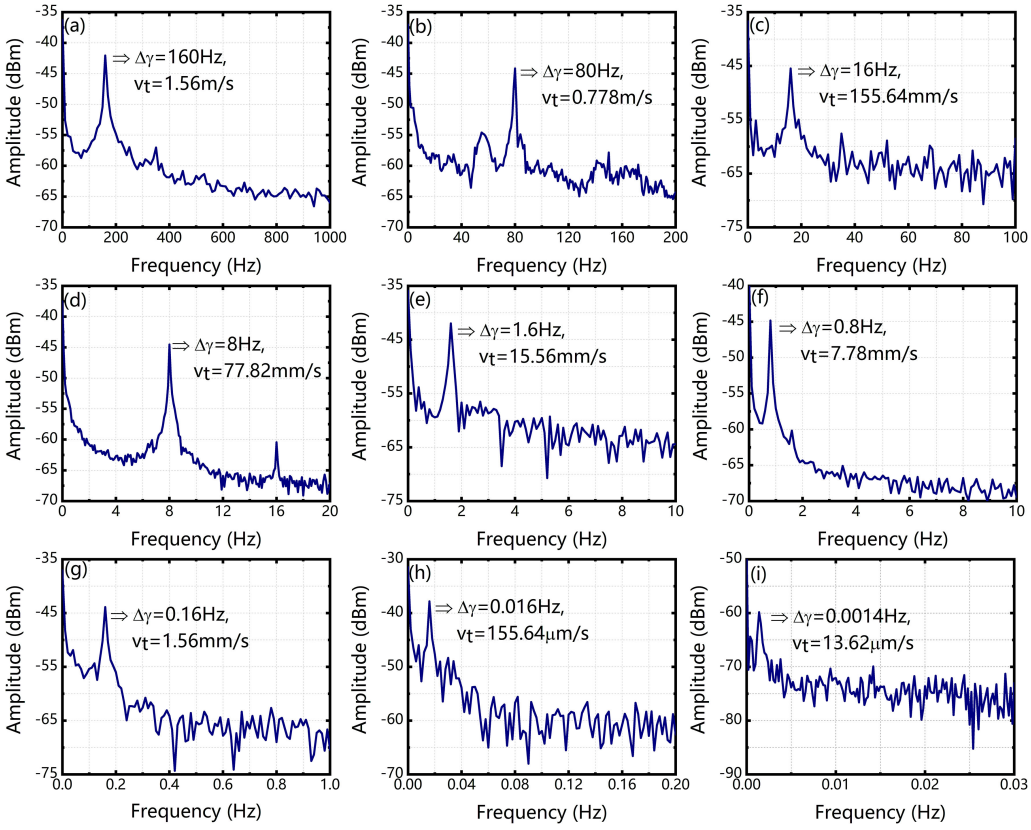

Fig. 7. The electronic spectra of the signals with different target speeds obtained by FFT. (a) setup velocity $v_s = 1.57$ m/s; (b) setup velocity $v_s = 0.775$ m/s; (c) setup velocity $v_s = 156.88$ mm/s; (d) setup velocity $v_s = 77.79$ mm/s; (e) setup velocity $v_s = 15.69$ mm/s; (f) setup velocity $v_s = 7.88$ mm/s; (g) setup velocity $v_s = 1.58$ mm/s; (h) setup velocity $v_s = 154.68$ μm/s; (i) setup velocity $v_s = 14.06$ μm/s.

the ML and SL. Fig. 5(b) shows the measured relationship between beat frequency and l_m with different l_s. The tunable range of the beat frequency is from 14.4 GHz to 40 GHz.

Fig. 6 shows the waveform obtained by the real time oscilloscope (OSC), which is the superposition of $l_1(t)$ and $l_2(t)$. According to Eq. (6), the frequency of the signal envelope (i.e., the red line) equals to $\Delta\gamma = \gamma_2 - \gamma_1$. The waveform data are sent to a computer and analyzed by fast Fourier transform (FFT). The precise value $\Delta\gamma$ is achieved by processing the FFT data. According to Eq. (7), we can calculate the velocity of the moving target. Fig. 7 shows the spectra of the waveform data under different speeds achieved by the FFT method. The speeds are also calculated according to

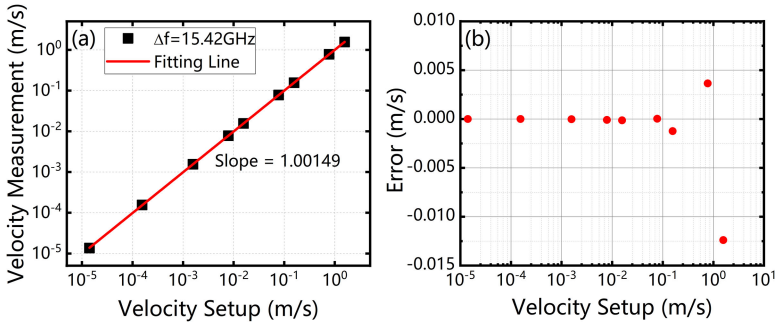

Fig. 8. (a) The fitting line of measurement velocity and setup velocity, the slope is 1.00149 and (b) the velocity error of the setup velocity when $\Delta f = 15.42$ GHz.

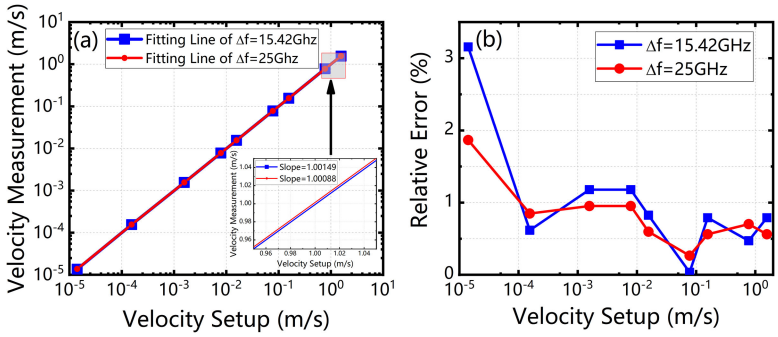

Fig. 9. (a) The measurement velocity fitting line when $\Delta f = 15.42$ GHz and $\Delta f = 25$ GHz, the slopes are respectively, 1.00149 and 1.00088. (b) The relative error of the measurement when the $\Delta f = 15.42$ GHz and $\Delta f = 25$ GHz.

the Eq. (7). The results illustrate that the speed measurement range is from 1.56 m/s to 13.62 μm /s, which covers 6 magnitudes. The measurement range of the DFDL is restricted by the target using in the experimental setup, which can be improved further in the future and even much smaller velocity can be monitored.

Fig. 8 shows the comparing result of measurement velocities and setup velocities. In Fig. 8(a), the setup velocities and measurement velocities are linearly fitted. Theoretically, the closer the slope is to 1, the higher the accuracy of the DFDL system is. The slope of the line is 1.00149, which means the measurement velocities deviation of the DFDL system is small. The Fig. 8(b) shows the measurement error versus the setup velocity. The absolute value of the maximum error and minimum error are 12.39 mm/s and 0.44 μm/s for the set velocity of 1.57 m/s and 14.06 μm/s respectively. The result shows that the whole DFDL system has great accuracy in the velocity measurement across the whole measuring range.

The measurement error is an important figure of merit for DFDL. It is well know that the measurement error is interrelated to the frequency of the beat signal. The higher the beat frequency, the smaller the measurement error [16]. In order to reduce the measurement error, we tune the beat frequency from 15.42 GHz to 25 GHz. According to Fig. 5(b), the beat frequency equals to 25 GHz, when $I_m = 60$ mA and $I_s = 55$ mA.

Fig. 9(a) shows the fitting lines of measurement results with different beat frequency at the same actual target velocity. The slopes are respectively 1.00149 and 1.00088 when $\Delta f = 15.42$ GHz and $\Delta f = 25$ GHz. It can be inferred that the DFDL system has better accuracy when $\Delta f = 25$ GHz. The measurement relative errors are shown in Fig. 9(b), and the largest error for $\Delta f = 15.42$ GHz and $\Delta f = 25$ GHz is 3.16% and 1.87% respectively. Here, the relative error is defined as the ratio of

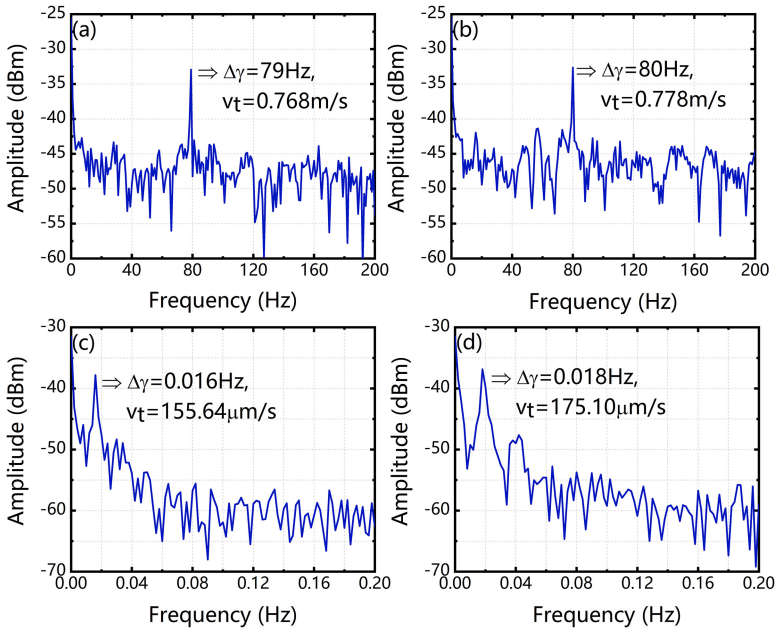

Fig. 10. The high resolution of the DFDL system. (a) and (b): velocity resolution is 9.73 mm/s, frequency resolution is 1 Hz; (c) and (d): velocity resolution is 19.46 μm/s, frequency resolution is 2 mHz.

the measurement error and the actual velocity. It is inferred from the results that the measurement errors are reduced when the beat frequency increases from 15.42 GHz to 25 GHz.

The resolution of the DFDL is determined by the linewidth of the beat signal and the frequency resolution of the FFT. Due to the injection of the RF signal, the linewidth of the beat signal is narrowed dramatically. Consequently, the measurement resolution of the proposed DFDL is mainly affected by the frequency resolution of the FFT which is determined by the time length of waveform data (as shown in Fig. 6). Fig. 10 shows the resolution of the DFDL system with different frequency resolution. The velocity resolution between Fig. 10(a) and Fig. 10(b) is 10 mm/s, when the frequency resolution is 1 Hz. Similarly, the velocity resolution of Fig. 10(c) and Fig. 10(d) is 19.46 μm/s, when the frequency resolution is 2 mHz. The velocity resolution can be further improved by increasing the time length of the waveform data. The results illustrate that the DFDL system is suitable to detect micro changes of the target velocity.

4. Conclusions

In summary, we demonstrate a simple and cost-effective DFDL utilizing a monolithic integrated two-section DFB laser as the dual-frequency light source. The measurement range is from 1.56 m/s to 13.62 μm/s, with the largest relative error of 3.16%. The DFDL measurement system can detect the subtle change of velocity at the minimum resolution of 1.95 μm/s, which has no correlation with the measured speed. The proposed DFDL is an ideal method to monitor target with very low speed.

References

[1] K. Rydhmer and A. Strand, "Applied hyperspectral LIDAR for monitoring fauna dispersal in aquatic environments," M.S. thesis, Dept. Math. Sci., Phy., Lund Univ., Lund, Sweden, 2016.
[2] W. Y. Yan, A. Shaker, and N. El-Ashmawy, "Urban land cover classification using airborne LiDAR data: A review," *Remote Sens. Environ.*, vol. 158, pp. 295–310, 2015.
[3] A. Dolfi-Bouteyre *et al.*, "Pulsed 1.5-μ m LIDAR for axial aircraft wake vortex detection based on high-brightness large-core fiber amplifier," *IEEE J. Sel. Topics Quantum Electron.*, vol. 15, no. 2, pp. 441–450, Mar./Apr. 2009.

[4] J. Vaughan, "Coherent laser spectroscopy and Doppler lidar sensing in the atmosphere," *Physica Scripta*, vol. 1998, no. T78, 1998, Art. no. 73.
[5] A. Fackelmeier, C. Morhart, and E. Biebl, "Dual frequency methods for identifying hidden targets in road traffic," in *Proc. Adv. Microsyst. Automot. Appl.*, 2008, pp. 11–20.
[6] L. Morvan *et al.*, "Building blocks for a two-frequency laser lidar-radar: A preliminary study," *Appl. Opt.*, vol. 41, no. 27, pp. 5702–5712, 2002.
[7] R. Kliese and A. Rakić, "Spectral broadening caused by dynamic speckle in self-mixing velocimetry sensors," *Opt. Express*, vol. 20, no. 17, pp. 18757–18771, 2012.
[8] U. Sharma, G. Chen, J. U. Kang, I. Ilev, and R. W. Waynant, "Fiber optic confocal laser Doppler velocimeter using an all-fiber laser source for high resolution measurements," *Opt. Express*, vol. 13, no. 16, pp. 6250–6258, 2005.
[9] W. L. Eberhard and R. M. Schotland, "Dual-frequency Doppler-lidar method of wind measurement," *Appl. Opt.*, vol. 19, no. 17, pp. 2967–2976, 1980.
[10] S. Matrosov, "Possibilities of cirrus particle sizing from dual-frequency radar measurements," *J. Geophys. Res., Atmos.*, vol. 98, no. D11, pp. 20675–20683, 1993.
[11] M. Shangguan *et al.*, "Dual-frequency Doppler lidar for wind detection with a superconducting nanowire single-photon detector," *Opt. Lett.*, vol. 42, no. 18, pp. 3541–3544, 2017.
[12] L. Morvan *et al.*, "Building blocks for a two-frequency laser lidar-radar: A preliminary study," *Appl. Opt.*, vol. 41, no. 27, pp. 5702–5712, 2002.
[13] C.-H. Cheng, C.-W. Lee, T.-W. Lin, and F.-Y. Lin, "Dual-frequency laser Doppler velocimeter for speckle noise reduction and coherence enhancement," *Opt. Express*, vol. 20, no. 18, pp. 20255–20265, 2012.
[14] D. Onori, F. Scotti, M. Scaffardi, A. Bogoni, and F. Laghezza, "Coherent interferometric dual-frequency laser radar for precise range/Doppler measurement," *J. Lightw. Technol.*, vol. 34, no. 20, pp. 4828–4834, Oct. 2016.
[15] R. Diaz, S.-C. Chan, and J.-M. Liu, "Lidar detection using a dual-frequency source," *Opt. Lett.*, vol. 31, no. 24, pp. 3600–3602, 2006.
[16] V. Vercesi, D. Onori, F. Laghezza, F. Scotti, A. Bogoni, and M. Scaffardi, "Frequency-agile dual-frequency lidar for integrated coherent radar-lidar architectures," *Opt. Lett.*, vol. 40, no. 7, pp. 1358–1361, 2015.
[17] C.-H. Cheng, L.-C. Lin, and F.-Y. Lin, "Self-mixing dual-frequency laser Doppler velocimeter," *Opt. Express*, vol. 22, no. 3, pp. 3600–3610, 2014.
[18] Y. Zhang *et al.*, "Modulation properties enhancement in a monolithic integrated two-section DFB laser utilizing side-mode injection locking method," *Opt. Express*, vol. 25, no. 22, pp. 27595–27608, 2017.
[19] Y. Dai and X. Chen, "DFB semiconductor lasers based on reconstruction-equivalent-chirp technology," *Opt. Express*, vol. 15, no. 5, pp. 2348–2353, 2007.
[20] J. Lu, S. Liu, Q. Tang, H. Xu, Y. Chen, and X. Chen, "Multi-wavelength distributed feedback laser array with very high wavelength-spacing precision," *Opt. Lett.*, vol. 40, no. 22, pp. 5136–5139, 2015.